Open access • Journal Article • DOI:10.1021/JACS.8B13898

"Dual-Key-and-Lock" Ruthenium Complex Probe for Lysosomal Formaldehyde in Cancer Cells and Tumors — Source link

Chaolong Liu, Run Zhang, Wenzhu Zhang, Jianping Liu ...+5 more authors

Institutions: Dalian University of Technology, University of Queensland, Stanford University

Published on: 29 Mar 2019 - Journal of the American Chemical Society (American Chemical Society)

Topics: Formaldehyde

A "Dual-key-and-lock" Ruthenium Complex Probe for Lysosomal Formaldehyde in Cancer Cells and Tumors

Chaolong Liu,[†] Run Zhang,[‡,*] Wenzhu Zhang,[†,*] Jianping Liu,[‡] Yong-Lei Wang,[⊥] Zhongbo Du,[†] Bo Song,[†] Zhi Ping Xu,[‡] Jingli Yuan[†,*]

[†] State Key Laboratory of Fine Chemicals, School of Chemistry, Dalian University of Technology, Dalian 116024, China.

[‡] Australian Institute for Bioengineering and Nanotechnology, The University of Queensland, St. Lucia, QLD 4072, Australia.

[⊥] Department of Chemistry, Stanford University, Stanford, California 94305, United States.

KEYWORDS. Ruthenium complex, dual-key-and-lock probe, formaldehyde, lysosome, cancer.

ABSTRACT: Biomedical investigations reveal that excessive formaldehyde generation is possibly a critical factor for tissue cancerization, cancer progression and metastasis. Responsive molecular probes that can detect lysosomal formaldehyde in live cells and tumors and monitor drug-triggered formaldehyde scavenging contribute potentially to future cancer diagnosis and treatment monitoring. Herein, a novel "dual-key-and-lock" strategy-based ruthenium(II) complex probe, **Ru-FA**, is reported as an effective tool for formaldehyde detection *in vitro* and *in vivo*. **Ru-FA** shows weak luminescence due to photon-induced electron transfer (PET) process from Ru(II) centre to electron withdrawing group 2,4-dinitrobenzene (DNB). Triggered by the specific reaction with formaldehyde (first "key") in an acidic microenvironment (second "key"), DNB is cleaved from **Ru-FA**, affording an emissive Ru(II) complex derivative, **Ru-NR**. Spectrometric analysis including steady-state and time-gated luminescence indicates that **Ru-FA** is favourable to be used as the probe for quantification of formaldehyde in human sera and mouse organs. **Ru-FA** is biocompatible and cell membrane permeable. Together with its smart "dual-key-and-lock" response to formaldehyde, luminescence imaging of lysosomal formaldehyde in live cells, visualization of tumor-derived endogenous formaldehyde and monitoring of formaldehyde scavenging in mice were achieved, followed by the successful demonstration on detection of formaldehyde in tumors and other organs. These *in vivo* and *in vitro* detection confirm not only the excessive formaldehyde generation in tumors, but also the efficient drug administration to scavenge formaldehyde, demonstrating the potential application of **Ru-FA** in cancer diagnosis and treatment monitoring through lysosomal formaldehyde detection.

INTRODUCTION

Although formaldehyde is a highly toxic compound and carcinogen to living organisms,[1] recent studies reveal the existence of endogenous formaldehyde at a higher concentration level in live cells, especially in cancer cells.[2-3] The concentration level of endogenous formaldehyde is ranged of 100-400 μM in cells, and around 100 μM in blood.[3-4] As one of the most important reactive carbonyl species (RCS), formaldehyde participates in various carbon cycles of intracellular metabolisms, and is implicated in a variety of human diseases.[3] Clinical data suggest that the endogenous formaldehyde concentration in cancer patient tissues is approximately 2-8 fold higher than that in adjacent tissues.[2] The elevated formaldehyde in cancer tissues is possibly a critical factor in tissue cancerization and tumor progression.[2, 5] At a single cell level, increasing evidences in recent investigations reveal that the biological roles of endogenous formaldehyde in live cells heavily rely on its generation and metastasis in lysosomes where majority of enzymes coexist in this acidic microenvironment (lysosomal pH_l 4.5-6.0).[2] Therefore, investigating the generation and the physiological functions of lysosomal formaldehyde in live cells and tumors is of great significance, which however remains a challenge because of the lack of robust bioanalytical methods.

Among various analytical methods, optical technique using responsive probes has previously been demonstrated its huge potentials in sensing and imaging of various biomarkers in living intact cells and organisms.[6-10] For formaldehyde analysis, several organic dye-based fluorescence probes were recently reported based on the exploitation of either formaldehyde-triggered 2-aza-Cope rearrangement reaction[11-23] or formaldehyde-amine condensation reaction.[24-31] Of these promising methods, few of probes could be used for detection and imaging of lysosomal formaldehyde in live cells,[32-34] and visualization and monitoring of tumor-derived formaldehyde. To unveil the biological functions of lysosomal formaldehyde in cancers,

the design of a responsive probe is expected to meet following criteria: i) abundant photo-chemical/physical properties allowing reliable formaldehyde analysis; ii) smart sensing mechanism facilitating "OFF-ON" luminescence response towards formaldehyde; iii) ability to detect and visualize formaldehyde expression in lysosomes specifically; and iv) ability to effectively detect and visualize tumor-derived endogenous formaldehyde as well as to monitor the formaldehyde scavenging effect of exogenous drug administration.

Generally, the probes for formaldehyde are designed by a "one-key-and-lock" strategy, *i.e.*, the quenched emission of the probe is switched on by reacting with formaldehyde (one "key").[17, 31] With this strategy for the detection and visualization of lysosomal formaldehyde, morpholine moiety is commonly conjugated to guide the original probe and also the products of original probe reacted with formaldehyde to be accumulated in lysosomes.[32, 34-37] Another design strategy, namely "dual-key-and-lock" system, has rarely been used for the development of probes for formaldehyde detection, but is more specific for lysosomal formaldehyde detection.[33, 38] With this strategy, the emission of the probe can only be switched on in the presence of both formaldehyde (first "key") and an acidic microenvironment (second "key"), precluding false positive signals derived from the probe being triggered "ON" in other organelles and then accumulated in lysosome (Scheme 1A).[38] Therefore, it is desirable to develop a new "dual-key-and-lock" strategy-based probe for the detection and monitoring of lysosomal formaldehyde in live cells and tumors.

In this contribution, a ruthenium(II) complex-based luminescence probe, **Ru-FA**, bearing a formaldehyde responsive linker is designed for the detection and visualization of lysosomal formaldehyde in cells as well as for the monitoring of tumor-derived endogenous formaldehyde in mice. **Ru-FA** is expected to be weakly luminescent due to the photoinduced electron transfer (PET) from Ru(II) center to electron withdrawing group, 2,4-dinitrobenzene (DNB) (Scheme 1B).[39] The reaction of **Ru-FA** with formaldehyde in acidic media leads to the cleavage of DNB to yield **Ru-NR**. It is thus envisioned that the Ru(II) complex luminescence can be switched on to allow quantitative formaldehyde detection. The response reaction has been confirmed by HRMS titration analysis, and the luminescence "OFF-ON" mechanism rationalized by theoretical computation. Formaldehyde detection in buffer and human sera, visualization of endogenous formaldehyde in lysosomes of live cells, tracing of cancer-derived endogenous formaldehyde and monitoring of formaldehyde scavenging in vivo have been successfully demonstrated.

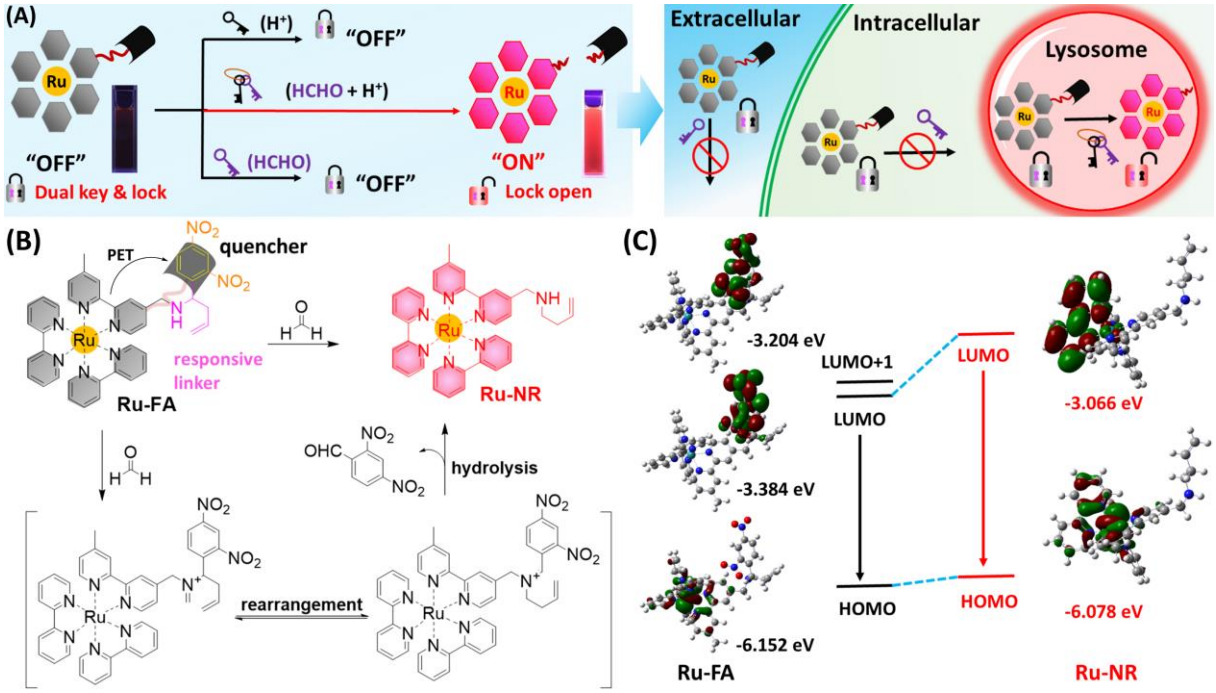

Scheme 1. (A) Schematic illustration of "dual-key-and-lock" ruthenium(II) complex probe for detection and imaging of lysosomal formaldehyde; (B) the reaction mechanism of **Ru-FA** with formaldehyde; (C) molecular orbitals (MO) of **Ru-FA** and **Ru-NR** corresponding to calculated emission transitions. The emission related computations were performed based on the optimized lowest-lying triplet excited states (T1) of Ru(II) complexes.

RESULTS AND DISCUSSION

Proposed response mechanism of Ru-FA towards formaldehyde. In continuation of our previous efforts on development and biological application of responsive metal complexes,[39-43] the present research focuses on the design and preparation of a Ru(II) complex-based probe for quantitative monitoring and imaging of cancer-derived endogenous formaldehyde in lysosomes of cancer cells and tumors. Robust luminescence properties of transition

metal complexes,[44-51] in particular Ru(II) complexes, provide a reliable platform for quantitative detection and imaging of formaldehyde *in vitro* and *in vivo*. The capability of lysosomal formaldehyde detection in cancer cells and tumors are secured by the "dual-key-and-lock" strategy. Together with the formaldehyde-triggered 2-aza-Cope rearrangement reaction, a unique probe, **Ru-FA**, is designed with a "luminophore-responsive linker-quencher" approach, i.e., incorporating the Ru(bipyridine)$_3^{2+}$ signaling unit with a DNB group through a formaldehyde responsive linker (Scheme 1B).

To gain initial information about luminescence properties of **Ru-FA** and **Ru-NR**, theoretical computations, i.e., density function theory (DFT) and time-dependent DFT (TD-DFT) calculations, were conducted. Corresponding transition energies of **Ru-FA** and **Ru-NR** and the rational of PET from Ru(II) centre to DNB moiety were investigated. As shown in Figure S1, S2, Table S1, and S2, the molecular geometries of **Ru-FA** and **Ru-NR** at ground state (S_0) and lowest-lying excited state (T_1) were optimized. The effects of bulk solvent (H_2O) are considered by means of the polarizable continuum model (PCM). Based on the S_0 molecular geometries (Figure S1, S2), molecular orbitals (MOs), including highest-occupied molecular orbitals (HOMOs) and lowest-unoccupied molecular orbitals (LUMOs) of both **Ru-FA** and **Ru-NR**, were calculated (Figures S3, S4). In **Ru-FA**, HOMOs (HOMO, HOMO-1, and HOMO-2) are mainly located on the Ru(II) centre; LUMOs (LUMO+2, LUMO+3, and LUMO+4) are largely distributed on bpy ligand. Interestingly, the LUMO and LUMO+1 clearly display DNB moiety character rather than whole bpy ligand. In **Ru-NR**, HOMOs are mainly distributed on the Ru(II) centre, and LUMOs are largely dominated on bpy ligand.

TD-DFT computations were then performed to investigate the electronic transitions that are related to their absorption profiles. As shown in Table S3, in **Ru-FA**, electronic transition from S_0 to first excited state (S_1) is mainly contributed by HOMO→LUMO (84.80%) and HOMO→LUMO+1 (14.68%). As the fact of the small oscillator strength (*f*) and the lack of overlap between the HOMO and LUMO, the $S_1 \leftarrow S_0$ is deemed a forbidden transition, i.e., S_1 state cannot be directly populated by photoexcitation but can be populated by internal conversion from higher excited states, such as S_{11}-S_{15}. ET character was noticed for S_1, S_2, S_3, S_6, S_8, S_9, and S_{10} for **Ru-FA**. In **Ru-NR**, characteristic ^{1}MLCT transitions were noticed for all excited singlet states (S_1-S_{10}).

The ET character and the luminescence "OFF-ON" response were then rationalized by TD-DFT calculations of the emission electronic transitions (Scheme 1C). These emission transitions were obtained based on the optimized molecular geometries of **Ru-FA** and **Ru-NR** at lowest-lying triplet excited states (T_1). As shown in Table S4, the T_1 of **Ru-FA** is largely contributed by HOMO→LUMO (68.11%) and HOMO→LUMO+1 (13.17%) with clear ET character. These computation data confirm that the luminescence quenching of **Ru-FA** is due to the PET process from Ru(II) centre to DNB moiety. For **Ru-NR**, the T_1 is mainly contributed by HOMO→LUMO (87.91%). This transition clearly showed ^{3}MLCT character that is normally featured by emissive transition of Ru(II) complexes. The calculated emission wavelength is 666 nm, which is in agreement with the spectrometric measurement emission of **Ru-NR** at 644 nm. On the basis of these calculations, the luminescence emission can be switched on when **Ru-FA** is transferred to **Ru-NR** by a specific formaldehyde and proton dually-driven reaction.

Ru-FA was synthesized through a three-step reaction procedure (Scheme S1). Briefly, compound **2** was firstly synthesized by reacting 2,4-dinitrobenzaldehyde with potassium allyltrifluoroborate, and further used as the reagent for the synthesis of the ligand FA-bpy (compound **4**). Then **Ru-FA** was synthesized by the coordination reaction between FA-bpy and *cis*-Ru(bpy)$_2$Cl$_2$·2H$_2$O in EtOH. The chemical structures of compound **2**, FA-bpy, **Ru-FA** and **Ru-NR** were characterized by ^{1}H NMR, ^{13}C NMR, ESI-MS, and elemental analysis (Figure S5-S14).

The reaction mechanism was verified by HRMS analysis of **Ru-FA** and formaldehyde solution of 50 mM NaAc-HAc buffer (pH 5.0). Upon addition of formaldehyde to the **Ru-FA** solution, peaks at m/z = 842.1752, 812.1639, 348.6049, 333.6000 were observed (Figure S15), which can be attributed to the species of [**Ru-NR**-PF$_6$+HCHO]$^+$ (calcd. m/z = 842.1745), [**Ru-NR**-PF$_6$]$^+$ (calcd. m/z = 812.1639), [**Ru-NR**-2PF$_6$+HCHO]$^{2+}$ (calcd. m/z = 348.6051) and [**Ru-NR**-2PF$_6$]$^{2+}$ (calcd. m/z = 333.5999), respectively. In another experiment, formaldehyde was added to **Ru-FA** solution in 50 mM NaAC-HAc buffer at pH 7.4. Peaks at m/z = 978.1649, 431.6047, 416.5999 were observed by HRMS analysis (Figure S16). These peaks can be attributed to the species of [**Ru-FA**-PF$_6$]$^+$ (calcd. m/z = 978.1654), [**Ru-FA**-2PF$_6$+HCHO]$^{2+}$ (calcd. m/z = 431.6059) and [**Ru-FA**-2PF$_6$]$^{2+}$ (calcd. m/z = 416.6006), indicating no reaction of formaldehyde with **Ru-FA** under neutral conditions.

UV-vis absorption spectra of both **Ru-FA** and **Ru-NR** showed visible absorption centred at 460 nm and UV absorption below 300 nm (Figure S17, Table S5), which can be ascribed to the characteristic metal-to-ligand charge transfer (MLCT) and the ligand-centred $\pi \rightarrow \pi^*$ transition, respectively.[52-54] Similar extinction coefficients (ε_{460nm}) were obtained for **Ru-FA** (1.20×10^4 cm^{-1} M^{-1}) and **Ru-NR** (1.19×10^4 cm^{-1} M^{-1}). Together with negligible changes of absorption spectra, the UV-vis absorption data corroborate the PET mechanism, in agreement with the theoretical computation result.

Upon excitation at 460 nm, **Ru-FA** and **Ru-NR** displayed maximum emissions at 634 nm and 644 nm (Figure S18), respectively. As anticipated, **Ru-FA** showed very weak luminescence (ϕ = 0.10%), while **Ru-NR** exhibited intense luminescence with a quantum yield of 2.12% (Table S5). These emission data indicate that the luminescence of **Ru-FA** can be switched on in the presence of formaldehyde due to the formation of **Ru-NR**. By a time-correlated single photon counting (TCSPC) technique, the emission lifetimes of **Ru-FA** and **Ru-NR** were determined to be 330.4

ns and 346.1 ns (Figure S19, Table S5), respectively. The long-lived emissions of these Ru(II) complexes contributed to the following time-gated luminescence (TGL) analysis of formaldehyde in human sera and mouse organ tissues.

Detection of formaldehyde with the probe Ru-FA. To validate the proposed "dual-key-and-lock" strategy, the effects of pH on the luminescence intensities of **Ru-FA** and **Ru-NR** and the luminescence response of **Ru-FA** towards formaldehyde were firstly investigated by spectrometric analysis. As shown in Figure 1A, the luminescence intensity of **Ru-FA** is weak and stable over a wide range of pH from 3.0 to 11.0. Upon addition of formaldehyde, no enhancement in luminescence intensity of the **Ru-FA** solution was observed in the pH range from 7.0 to 11.0, while significantly enhanced luminescence of **Ru-FA** solution was noticed in pH of 3.0 to 6.0. **Ru-NR** showed intense and stable luminescence emission in the pH range from 3.0 to 11.0, suggesting the sensing reaction between **Ru-FA** and formaldehyde happens in the acidic condition only.

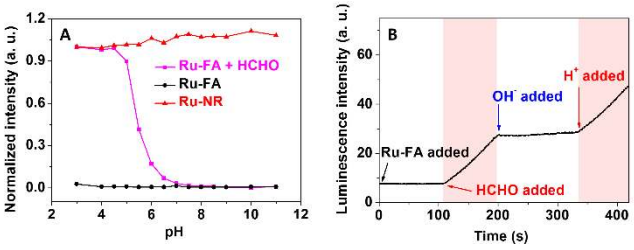

Figure 1. pH-dependent luminescence response of **Ru-FA** towards formaldehyde. (A) Effects of pH on the luminescence intensities of **Ru-FA** (10 μM) and **Ru-NR** (10 μM), and the response of **Ru-FA** (10 μM) towards formaldehyde (4 mM). (B) Real-time luminescence response of **Ru-FA** (20 μM) towards formaldehyde at different pH environments. To the solution of **Ru-FA** in 50 mM HOAc/OAc$^-$ buffer at pH 5.0 was added formaldehyde (final concentration 8 mM), then NaOH (3 M) and HCl (3 M) were added to adjust pH to 7.5 and 5.0, respectively. The transition between each regime is marked with an arrow. Excitation was performed at 460 nm.

To further confirm the pH-dependent sensing reaction, time-profile luminescence enhancement of **Ru-FA** solutions with different pH values was recorded in the presence of formaldehyde. As shown in Figure 1B, gradual enhancement in luminescence intensity at 644 nm was noticed in HOAc/OAc$^-$ buffered formaldehyde solution of pH 5.0. The increase was stopped immediately when the solution's pH was adjusted to neutral (pH 7.5), and then remained constant until the solution's pH was adjusted back to acidic (pH 5.0). These results reveal that **Ru-FA** responds to formaldehyde only in weakly acidic media, such as in the acidic lysosome (pH 4.5-6.0).[55]

Time-dependent luminescence enhancement profile of the **Ru-FA** (10 μM) solution was investigated by recording the changes of emission intensity at 644 nm in the absence and presence of formaldehyde. As shown in Figure S20, no change of luminescence intensity was noticed for **Ru-FA** solution in HOAc/OAc$^-$ buffer at pH 5.0. Upon addition of formaldehyde, the luminescence intensity was gradually increased and reached the maximum after 120 min reaction.

Figure 2A illustrates the emission spectrum changes of **Ru-FA** (10 μM) solutions with various concentrations of formaldehyde. The emission was clearly enhanced with the formaldehyde concentration (Figure 2B). The maximum luminescence intensity was reached in 4 mM formaldehyde solution. The luminescence intensity at 644 nm exhibited a good linear correlation with the concentration of formaldehyde (R^2 = 0.997) (Figure 2C). Based on the definition by IUPAC (3σ/k), the detection limit was determined to be 19.8 nM, indicating high sensitivity of **Ru-FA** to formaldehyde. Moreover, the paper-based formaldehyde test strips were prepared by dipping into **Ru-FA** solution and then air-drying. These test strips showed consistent luminescence color changes when they were contacted with different concentrations of formaldehyde (the inset in Figure 2B), suggesting the potential of **Ru-FA** for the paper-based analysis of soluble formaldehyde.

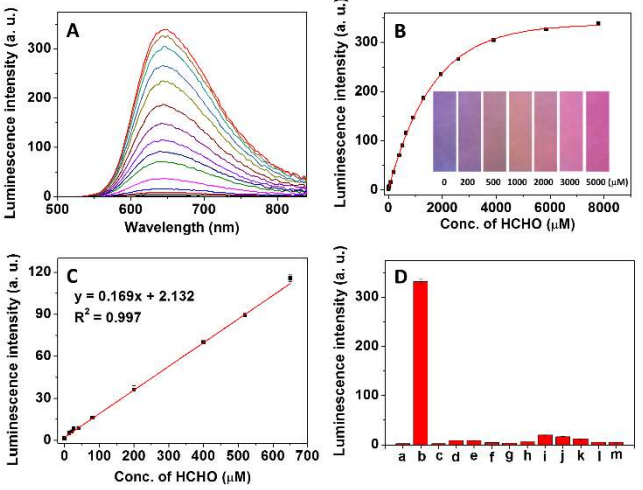

Figure 2. Luminescence response of **Ru-FA** towards formaldehyde in 50 mM HOAc/OAc$^-$ buffer at pH 5.0. (A) Emission spectra of **Ru-FA** (10 μM) in the presence of formaldehyde at different concentrations; (B) correlation of luminescence intensity at 644 nm to the concentration of formaldehyde (inset: visual photoluminescence colors of the **Ru-FA**-loaded filter paper strips treated with various concentrations of formaldehyde); (C) linear correlation of luminescence intensity to the concentration of formaldehyde in the range of 0 to 650 μM; (D) luminescence intensities at 644 nm of the **Ru-FA** solution (10 μM) upon reactions with various relevant molecules and ions (4 mM): a) blank; b) formaldehyde; c) acetaldehyde; d) pyruvaldehyde; e) benzaldehyde; f) glyoxal; g) glucose; h) GSH; i) Cys; j) Hcy; k) His; l) H_2S; m) H_2O_2. Excitation was performed at 460 nm.

The specificity of luminescence response of **Ru-FA** towards formaldehyde is shown in Figure 2D. The emission intensity at 644 nm did not change upon additions of acetaldehyde, pyruvaldehyde, benzaldehyde, glyoxal, glucose, glutathione (GSH), cysteine (Cys), homocysteine (Hcy),

histidine (His), H_2S, and H_2O_2 at the concentration of 4 mM. In sharp contrast, a remarkable enhancement in luminescence intensity was obtained after **Ru-FA** was reacted with formaldehyde, indicating high selectivity of **Ru-FA** for formaldehyde detection.

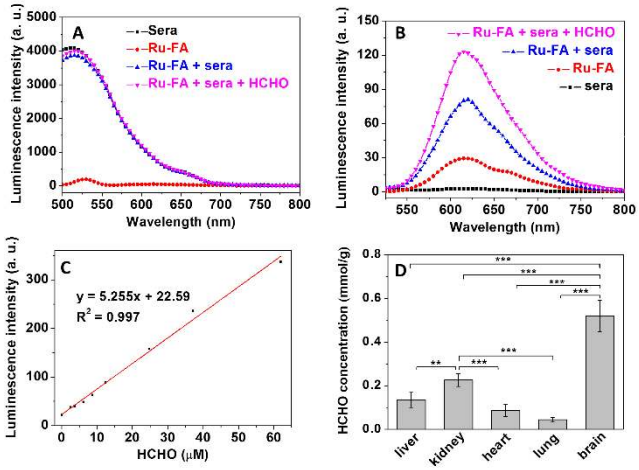

Figure 3. Luminescence (A, 0 ns delay) and time-gated luminescence (B, 100 ns delay) spectra of human serum samples (10-fold diluted with 50 mM HOAc/OAc⁻ buffer of pH 5.0) before and after reacting with **Ru-FA** (the concentration of exogenous formaldehyde used for the detection was 8.86 μM). (C) Linear correlation of time-gated luminescence intensity to the concentration of formaldehyde in the range of 0 to 60 μM. (D) Time-gated luminescence analysis results of formaldehyde concentrations in ex vivo dissected organs of a mouse. Excitation was performed at 450 nm.

Ru-FA was found to able to quantify the formaldehyde level in human serum samples in combination with the time-gated luminescence analysis (TGLA) (Figure 3). Intense background autofluorescence was noticed even after 10-fold dilution of sera with 50 mM HOAc/OAc⁻ buffer (pH 5.0) (Figure 3A). With additions of **Ru-FA** and exogenous formaldehyde into the sera, the emission spectrum (0 ns delay) remained no changes. In contrast, this background autofluorescence was completely removed in the TGLA mode (100 ns delay) (Figure 3B). The TGL spectral intensity significantly increased with addition of **Ru-FA** into the sera, which can be attributed to the response of **Ru-FA** towards formaldehyde in sera. Furthermore, the TGL intensity of the sera increased by adding exogenous formaldehyde. The TGL intensity showed a linear correlation to the concentration of formaldehyde (Figure 3C). According to this standard curve, the concentration level of formaldehyde in human sera was calculated to be 106.2 ± 1.9 μM, which is in consistent with the results reported in the literature.[2, 5] Consistently, the TGLA of the formaldehyde level in artificial spiked human serum samples exhibited recovery of 90.2% to 91.4% (Table S6). Altogether these results demonstrate that **Ru-FA** can serve as a TGL probe for quantifying formaldehyde in human sera with a high accuracy.

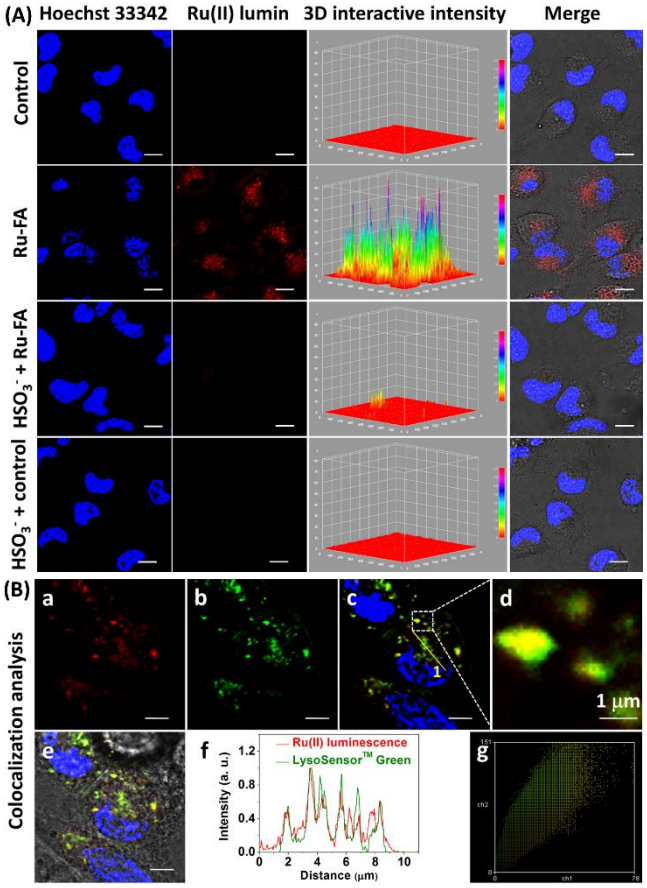

Figure 4. Luminescence imaging of endogenous formaldehyde in lysosomes of live HeLa cells. (A) Luminescence imaging of endogenous formaldehyde in live HeLa cells (scale bar: 10 μm). Control group: the cells were stained by Hochest 33342 only; **Ru-FA** group: the cells were incubated with **Ru-FA** (10 μM) for 4 h, and then stained by Hochest 33342; HSO_3^-+**Ru-FA** group: the cells were pre-treated with $NaHSO_3$ (200 μM) for 0.5 h, and stained with **Ru-FA** (10 μM) for 4 h, and then stained by Hochest 33342; HSO_3^-+control group: the cells were treated with $NaHSO_3$ (200 μM) for 0.5 h, and then stained by Hochest 33342. (B) Intracellular colocalization analysis of **Ru-FA** and LysosensorTM Green in live HeLa cells (scale bar: 5 μm). The cells were incubated with 10 μM **Ru-FA** for 4 h, and then stained with LysosensorTM Green and Hochest 33342. (a) the image of red emission channel; (b) the image of green emission channel; (c) merged image of (a), (b) and Hoechst 33342-stained nucleus; (d) zoom-in of the interested area in (c); (e) merged image of (c) and corresponding bright-field image; (f) luminescence intensity profile of the regions of interest (ROIs) across HeLa cells in (c); (g) intensity correlation plot of HeLa cells that were co-stained with **Ru-FA** and LysoSensor™ Green.

Moreover, the formaldehyde concentration in different mouse organs was quantified. The collected mouse organs were homogenized and then measured with the **Ru-FA** probe. As shown in Figure 3D, the formaldehyde concentration is 0.135 mmol/g in liver, 0.226 mmol/g in kidney, 0.0864 mmol/g in heart, 0.0447 mmol/g in lung, and 0.519

mmol/g in brain, respectively. The higher concentration of endogenous formaldehyde in brain may contribute to the various activities, such as memory and cognition processes.[56]

Visualization of lysosomal formaldehyde in cells. **Ru-FA** and **Ru-NR** did not show acute cytotoxicity determined by MTT analysis. Cell viability remained more than 80% after incubation of cells (HeLa, MCF-7, and RAW 264.7 macrophage) with either **Ru-FA** (50 μM) or **Ru-NR** (50 μM) containing media for 24, 48, and 72 h (Figure S21). For another degradation product of **Ru-FA** reacting with formaldehyde, 2,4-dinitrobenzaldehyde, MTT cytotoxicity analysis showed > 80% and > 70% HeLa cell viability after 24 and 72 h incubation, respectively. Therefore, **Ru-FA** and the degradation products, **Ru-NR** and 2,4-dinitrobenzaldehyde have low cytotoxicity to cells under experimental conditions (10 μM for 4 h incubation).

To evaluate the feasibility of **Ru-FA** for specific luminescence visualization of lysosomal formaldehyde, HeLa cells were incubated in 10 μM **Ru-FA** media for 4 h. In another group, HeLa cells were pre-treated with $NaHSO_3$ (formaldehyde scavenger)[31] for 30 min, and then stained with 10 μM **Ru-FA**. As shown in Figure 4A, HeLa cells in the control group (stained by Hochest33342 only) did not show any red luminescence, while clearly red intracellular luminescence were observed after staining with **Ru-FA**. The $NaHSO_3$ pre-treated HeLa cells showed remarkably weak red luminescence. Considering that there is a high level of endogenous formaldehyde in cancer cells, these cell images suggest the feasibility of **Ru-FA** for imaging endogenous formaldehyde in live cells.

The **Ru-FA** stained HeLa cells were then incubated with commercially available Lysosensor™ Green, and subjected to microscopy luminescence imaging analysis. Bright yellow luminescence was noticed from the merged image of HeLa cells (Figure 4B(c, d)). The luminescence intensity profile in the line regions of interest (ROI 1 in Figure 4B(c)) across the HeLa cells shows the similarity in green and red channels (Figure 4B(f)). Quantitatively, the intensity correlation is also reflected by the large Pearson's coefficient (0.969) and Mander's overlap coefficient (0.937), indicating a high colocalization of Ru(II) complex and Lysosensor™ Green in the subcellular apartment. Because the probe **Ru-FA** can only respond to formaldehyde in the acidic microenvironment, the images clearly demonstrate that only lysosomal formaldehyde in live HeLa cells was visualized.

To further confirm luminescent **Ru-NR** production in lysosomes of live cells, time course luminescent imaging of the **Ru-FA**-stained HeLa cells was carried out. As shown in Figure S22, intracellular luminescence increase of red channel (**Ru-FA** channel) was observed, indicating that

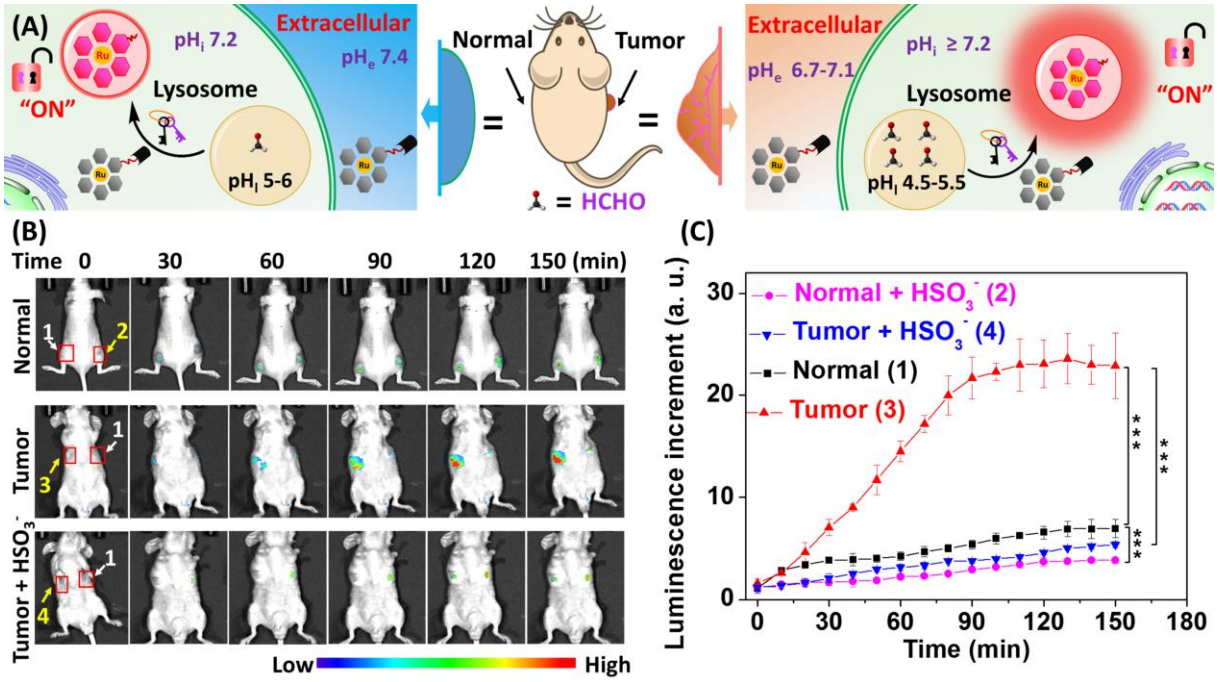

Figure 5. Monitoring of tumor-derived endogenous formaldehyde in nude mice. (A) Schematic illustration for visualizing endogenously lysosomal formaldehyde in normal and tumor tissues of mice using **Ru-FA** as a probe. (B) Imaging of endogenous formaldehyde in live mice with different treatments. 1) Saline (50 μL) was subcutaneously injected into mice (left hind limb for normal mice; right axillae for tumor bearing mice), followed by the injection of **Ru-FA** (70 μL, 300 μM) into the same area; 2) $NaHSO_3$ (50 μL, 500 μM) was subcutaneously injected into mice, followed by the injection of **Ru-FA** (70 μL, 300 μM) into the same area; 3) **Ru-FA** (70 μL, 300 μM) was injected into the tumor; 4) $NaHSO_3$ (50 μL, 500 μM) was injected into the tumor, followed by the injection of **Ru-FA** (70 μL, 300 μM) into the same area. (C) Time-dependent luminescence intensity enhancement of mice in (B).

Ru-FA responds to endogenous formaldehyde in live cells to form luminescent **Ru-NR**. Co-staining with LysoSensor™ Green, luminescence images showed well colocalisation of signals from green and red channels. Moreover, red luminescence signals were only found within lysosomes during co-incubation of HeLa cells with **Ru-FA** for 1-4 h (1 h interval), corroborating that **Ru-NR** is generated after the reaction of **Ru-FA** with formaldehyde in lysosomes of live cells.

Monitoring of tumor-derived lysosomal formaldehyde. Capability of **Ru-FA** for tracing tumor-derived lysosomal formaldehyde and further monitoring the formaldehyde scavenging was evaluated by *in vivo* and *ex vivo* imaging analysis. Proof-of-concept experiments were initially performed by imaging the endogenous formaldehyde in normal (non-tumor) mice. Buffers (50 μL) with different pH values were subcutaneously injected into mouse hind limbs, followed by the injection of **Ru-FA** into the same area. Images in Figure S23 show gradually increased luminescence intensities for both hind limbs. Pre-injection with HOAc/OAc^- buffer (pH 5.0) allowed the temporal decrease of local pH at right hind limb. Relatively fast luminescence response and higher luminescence intensity were thus observed from right hind limb because the injected **Ru-FA** responded to both extracellular and intracellular formaldehyde in this artificial acidic microenvironment.

Another group of experiment was performed to confirm the feasibility of **Ru-FA** for monitoring the scavenging of formaldehyde by $NaHSO_3$ injection at right hind limb of normal mice. As shown in Figures 5B, 5C, and S24, the luminescence intensity of control group (area "1", **Ru-FA** injection only) was significant higher than the one that pretreated with $NaHSO_3$ (area "2"). Lower luminescence intensity at area "2" could be attributed to the scavenging of endogenous formaldehyde by $NaHSO_3$. The images indicate that **Ru-FA** can be used as a luminescence probe for *in vivo* visualization of endogenous formaldehyde.

Visualization of cancer tissue-derived endogenous formaldehyde in tumor-bearing mice was demonstrated by using **Ru-FA** as a probe (Figures 5, S25). **Ru-FA** was injected into the tumor (area "3"), and then the luminescence image was recorded in every 10 min within 150 min. Rapid luminescence enhancement was clearly observed and the luminescence intensity reached a maximum at approximate 100 min post injection (Figure 5C). Comparing of the luminescence intensity at normal tissue (area "1" in middle row of Figure 5B), significant luminescence increase was observed from tumor tissue. Imaging analysis showed 3.7-fold luminescence enhancement at 100 min (Figure 5C). The fast luminescence increment and higher intensity of tumor tissue could be ascribed to: i) higher level of tumor-derived endogenous formaldehyde; and ii) lower lysosomal pH level in tumor tissue cells (pH 4.5-5.0) than normal tissue cells (pH 5.0-6.0) (Figure 5A).[55]

Then, the ability of **Ru-FA** for monitoring the formaldehyde scavenging in tumor-bearing mice was evaluated. Tumor (area "4") was pre-treated with $NaHSO_3$, followed by the injection of **Ru-FA** and luminescence imaging in every 10 min. As shown in Figures 5, and S26, $NaHSO_3$ pre-treated tumor showed weak luminescence over the time of

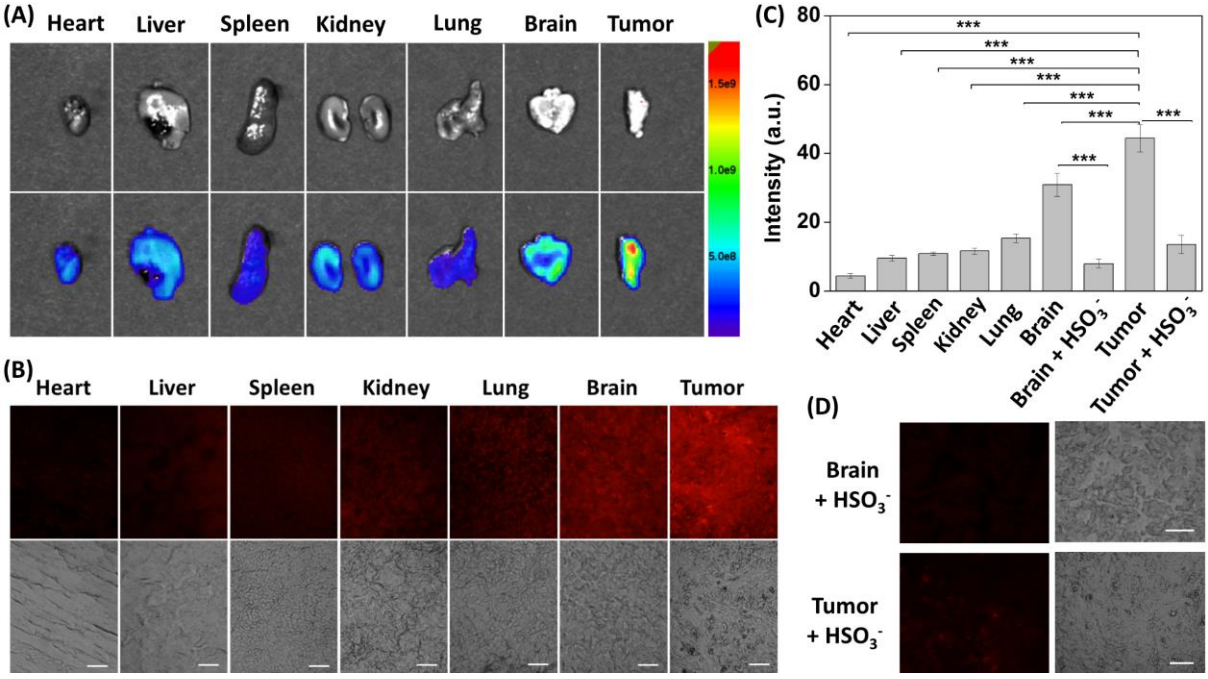

Figure 6. (A) Visualization of endogenous formaldehyde in intact organs of a mouse, including heart, liver, spleen, kidney, lung, brain and tumor. (B) Luminescence imaging of endogenous formaldehyde in the mouse organ tissue slices. (C) Mean luminescence intensity for each of the mouse tissue slices. (D) Brain and tumor tissue slices were pretreated with $NaHSO_3$, and then stained with **Ru-FA**. Scale bar: 100 μm.

0-150 min. More than 4.2-fold decreased luminescence intensity was noticed compared to that observed from the $NaHSO_3$-untreated tumor. This significant luminescence decrease can be attributed to the low formaldehyde concentration after $NaHSO_3$ scavenging, indicating the potential of **Ru-FA** for assessing formaldehyde-mediated tumor progression.

By using **Ru-FA** as a probe, corroborating evidence of the higher tumor-derived formaldehyde concentration was provided by *ex vivo* luminescence imaging analysis. The mouse was sacrificed, and its organs were collected. After being incubated with **Ru-FA** in 50 mM HOAc/OAc^- buffer at pH 5.0, luminescence images of the organs were recorded. As shown in Figure 6A, the highest luminescence signal was observed from tumor tissue, followed by the one from brain tissue. For the frozen sectioned organ tissue slices, red luminescence signal was noticed for all slices, and the most bright luminescence image was presented by the tumor tissue slice (Figure 6B). Mean luminescence intensity analysis reveals that the brightness of tumor tissue slice is significantly higher than other tissues (Figure 6C), corroborating the excessive formaldehyde production by tumor tissues. In agreement with the results of direct organ imaging and time-gated luminescence analysis (Figure 3D), significantly higher concentration of formaldehyde in brain was found than that in other organs except tumor (Figure S27), suggesting that brain is one of the major harbor for endogenous formaldehyde. By treating with $NaHSO_3$, weak luminescence was noticed in both tumor and brain tissues (Figure 6D) and thus significant decrease in intensity was observed (Figure 6C). Above *in vivo* and *ex vivo* images gave direct evidences for the excessive tumor-derived formaldehyde and the feasibility of tumor formaldehyde scavenging by drug administering. More importantly, these variations of formaldehyde level were exactly monitored by using **Ru-FA** as a probe, which highlights the potential of **Ru-FA** for the future investigation of formaldehyde-mediated tumor progression.

CONCLUSIONS

In the present study, a unique "dual-key-and-lock" Ru(II) complex probe, **Ru-FA**, has been developed for quantitative detection and imaging of lysosomal formaldehyde in cancer cells and tumors. As the result of PET process from Ru(II) centre to electron withdrawing moiety DNB, **Ru-FA** itself displays weak luminescence, but its emission can be significantly increased after reacting with formaldehyde (key "one") in acidic microenvironment (key "two"), accompanied by the production of emissive **Ru-NR**. Spectrometric analysis, including steady-state and time-gated luminescence analysis showed that **Ru-FA** is favorable to be used for detecting formaldehyde in buffer and human sera, as well as in mouse organs. **Ru-FA** shows low cytotoxicity and good cell membrane permeability. Together with the smart "dual-key-and-lock" response of **Ru-FA** towards formaldehyde, investigations of lysosomal formaldehyde and the capability of formaldehyde scavenging at cellular scale were achieved by imaging analysis. Using **Ru-FA** as a probe, visualization of tumor-derived endogenous formaldehyde and monitoring of formaldehyde scavenging by exogenous drug were successfully demonstrated. The mouse images strongly suggest that **Ru-FA** could be a straightforward tool for tracing the tumor-derived endogenous formaldehyde as well as for monitoring the formaldehyde scavenging, potentially contributing to future clinical or pre-clinical cancer early diagnosis and treatment response monitoring. It is also anticipated that the "dual-key-and-lock" design strategy could be an ideal strategy for promoting the development of responsive probes, especially transition metal complex-based luminescence probes for sensing and imaging of biomolecules.

EXPERIMENTAL SECTION

Syntheses of Ru-FA and Ru-NR. The synthesis procedure of compound 2, compound 4, **Ru-FA** and **Ru-NR** is illustrated in Scheme S1A. Specifically, the studies of **Ru-FA** probe for formaldehyde detection were based on a racemic mixture (*rac*-**Ru-FA**), including Δ-**Ru-FA** and Λ-**Ru-FA** enantiomers. The racemates, Δ-/Λ-**Ru-FA** enantiomers were synthesized by reacting of racemic *cis*-$[Ru(bpy)_2Cl_2]$ (bpy = 2,2'-bipyridine) with the ligand 4 (Scheme S1A). The Δ-/Λ-**Ru-NR** was synthesized by reacting of racemic **Ru-Br** with 3-butenylamine. The absolute configurations of the Δ-**Ru-FA** and Λ-**Ru-FA** enantiomers and the luminescent product Δ-**Ru-NR** and Λ-**Ru-NR** enantiomers were shown in Scheme S1B. To simplify the description, names of **Ru-FA** and **Ru-NR** were used throughout. The details for the synthesis of **Ru-FA** and **Ru-NR** are described as follows.

Synthesis of Compound 2. 2,4-Dinitrobenzaldehyde (0.114mmol, 22.3 mg) was added into 4 mL of NH_3 solution (7.0 M in methanol, 28 mmol). The mixture was stirred at 25 °C for 15 min before addition of potassium allyltrifluoroborate (0.34 mmol, 50 mg) and 20 μL of deionized water. The mixture was reacted at 30 °C for 16 h. The solvent was then evaporated by a rotary evaporator. The crude product was purified by column chromatography (silica gel) using dichloromethane/methanol (40:1 v/v) as the eluent. After evaporation, compound **2** was obtained as the white oil (19.4 mg, 72.1% yield). ^{1}H NMR (400 MHz, $CDCl_3$): δ (ppm) = 8.67 (s, 1H), 8.44 (d, *J* = 8.8 Hz, 1H), 8.15 (d, *J* = 7.2 Hz, 1H), 5.86-5.73 (m, 1H), 5.21-5.13 (m, 1H), 4.73-4.61 (m, 1H), 2.66-2.55 (m, 1H), 2.38-2.25 (m, 1H). ESI-MS (m/z): 238.02 ($[M+H]^+$).

Synthesis of Compound 4. Compound 2 (12.5 mg, 0.056 mmol), compound 3 (4-methyl-2,2'-bipyridyl-4'-carboxaldehyde) (21.0 mg, 0.106 mmol) and sodium cyanotrihydroborate (13.0 mg, 0.212 mmol) were dissolved in 5 mL of methanol. After the addition of 50 μL acetic acid, the mixture was reacted at 30 °C for 3 h. The solvent was evaporated, and the residue was purified by column chromatography (silica gel) using dichloromethane/methanol (50:1 v/v) as the eluent. The fraction containing compound 4 was collected and the eluent was evaporated to give the compound 4 as the yellow oil (16.5 mg, 70.0% yield). ^{1}H NMR (500 MHz, $CDCl_3$): δ (ppm) = 8.63 (s, 1H), 8.59 (d, *J* = 5.0 Hz, 1H), 8.55 (d, *J* = 5.0 Hz, 1H), 8.41 (d, *J* = 9.0 Hz, 1H),

8.26-8.21 (m, 2H), 8.18 (s, 1H), 7.18 (dd, *J* = 14.0 Hz, 5.0 Hz, 2H), 5.86-5.72 (m, 1H), 5.24-5.08 (m, 2H), 3.78-3.58 (m, 2H), 2.71-2.60 (m, 1H), 2.44 (s, 3H), 2.41-2.31 (m, 1H). ESI-MS (m/z): 420.25 ($[M+H]^+$).

Synthesis of the Probe Ru-FA. Compound 4 (83.8 mg, 0.2 mmol) and compound 5 (*cis*-$Ru(bpy)_2Cl_2{\cdot}2H_2O$) (146 mg, 0.2 mmol) were mixed in 20 mL of ethanol. Under an argon atmosphere, the mixture was refluxed overnight. After evaporation, the resulting product was purified by silica gel column chromatography using 10:1 (v/v) CH_3CN/H_2O (saturated KNO_3 aqueous solution) as the eluent. The fraction containing **Ru-FA** was collected and the eluent was evaporated. The purified product was added into 10 mL of acetonitrile, and excess potassium nitrate was isolated by filtration. The solvent was evaporated, and the product was dissolved in 3 mL H_2O. Then, saturated NH_4PF_6 aqueous solution (0.5 mL) was added into the solution to give **Ru-FA** as the red precipitate (201.0 mg, 89.5% yield). ^{1}H NMR (500 MHz, CH_3CN): δ (ppm) = 8.55-8.46 (m, 5H), 8.46-8.41 (m, 1H), 8.31-8.24 (m, 2H), 8.10 (d, *J* = 7.2 Hz, 1H), 8.08-8.01 (m, 4H), 7.76-7.65 (m, 4H), 7.59-7.54 (m, 1H), 7.53 (d, *J* = 4.4 Hz, 1H), 7.46-7.34 (m, 4H), 7.28-7.20 (m, 2H), 5.88-5.70 (m, 1H), 5.17-5.00 (m, 2H), 4.21 (t, *J* = 5.6 Hz, 1H), 3.87-3.68 (m, 2H), 2.58-2.49 (m, 5H). ^{13}C NMR (100 MHz, CD_3CN): 156.71, 156.43, 156.05, 151.39, 151.21, 151.09, 150.83, 150.52, 150.21, 149.63, 146.59, 144.61, 137.36, 133.67, 130.77, 127.23, 126.78, 126.36, 126.28, 123.92, 123.89, 123.00, 122.79, 119.09, 117.86, 56.14, 49.18, 41.24, 19.97. Elemental analysis calcd. (%) for $C_{42}H_{37}F_{12}N_9O_4P_2Ru{\cdot}0.4NH_4PF_6$: C 42.46, H 3.28, N 11.08; found (%): C 42.36, H 3.081, N 10.77. ESI-MS (m/z): 416.49 ($[M-2PF_6]^{2+}$), 978.30 ($[M-PF_6]^+$).

Synthesis of Ru-NR. **Ru-Br** (96.6 mg, 0.1 mmol), 3-butenylamine hydrochloride (10.7 mg, 0.1 mmol) and potassium carbonate (137.9 mg, 1 mmol) were mixed in 10 mL of acetonitrile. Under an argon atmosphere, the mixture was refluxed overnight. The solvent was then evaporated by a rotary evaporator, and crude product was purified by column chromatography (silica gel) using CH_3CN/H_2O (saturated KNO_3 aqueous solution, 15:1 v/v) as the eluent. The purified product was added into 10 mL of acetonitrile, and excess potassium nitrate was isolated by filtration. The solvent was evaporated, and the product was dissolved in 3 mL H_2O. Then, saturated NH_4PF_6 aqueous solution (0.5 mL) was added into the solution. **Ru-NR** was then obtained as the red solid (40.3 mg, 42.1% yield). ^{1}H NMR (400 MHz, CD_3CN): δ (ppm) = 8.59-8.44 (m, 5H), 8.34 (s, 1H), 8.13-8.00 (m, 4H), 7.83-7.66 (m, 5H), 7.57 (d, J = 6.0 Hz, 1H), 7.48-7.34 (m, 5H), 7.28 (d, J = 5.6 Hz, 1H), 5.88-5.72 (m, 1H), 5.18 (m, 2H), 4.28 (s, 2H), 3.12 (t, J = 7.2 Hz, 2H), 2.56 (s, 3H), 2.44 (q, J = 7.2 Hz, 2H). ^{13}C NMR (100 MHz, CD_3CN): 157.62, 157.05, 157.02, 156.91, 155.93, 152.06, 151.75, 151.66, 151.61, 151.45, 150.96, 150.71, 142.90, 137.85, 133.08, 128.76, 127.65, 127.59, 125.20, 124.52, 124.27, 118.30, 49.87, 47.78, 30.48, 20.35. Elemental analysis calcd. (%) for $C_{36}H_{36}F_{12}N_7P_2Ru{\cdot}PF_6$: C 39.21, H 3.29, N 8.89; found (%): C 39.87, H 3.19, N 9.03. HRMS (m/z): 333.5966 ($[M-2PF_6]^{2+}$), 812.1556 ($[M-PF_6]^+$).

ASSOCIATED CONTENT

Supporting Information. General Information, synthesis procedure and characterization of **Ru-FA**, theoretical computations and photophysical properties of **Ru-FA** and **Ru-NR**, detection of formaldehyde in buffer and biological samples, imaging of endogenous formaldehyde in mice. The Supporting Information is available free of charge via the Internet at http://pubs.acs.org

AUTHOR INFORMATION

Corresponding Author

* R. Zhang, Email: r.zhang@uq.edu.au
* W. Zhang, Email: wzhzhang@dlut.edu.cn
* J. Yuan, Email: jlyuan@dlut.edu.cn

Author Contributions

The manuscript was written through contributions of all authors. / All authors have given approval to the final version of the manuscript.

Notes

The authors declare no competing financial interests.

ACKNOWLEDGMENT

We gratefully acknowledge the financial supports from the National Natural Science Foundation of China (Grant Nos. 21475015, 21775015), Australian Research Council (DE170100092), and the National Health and Medical Research Council (APP1125794). The facilities and assistance of the Queensland Node of the Australian National Fabrication Facility (ANFF-Q), The University of Queensland, are also acknowledged.

REFERENCES

1. Bosetti, C.; McLaughlin, J. K.; Tarone, R. E.; Pira, E.; La Vecchia, C., Formaldehyde and cancer risk: a quantitative review of cohort studies through 2006. *Ann. Oncol.* **2008,** *19* (1), 29-43.
2. Pontel, Lucas B.; Rosado, Ivan V.; Burgos-Barragan, G.; Garaycoechea, Juan I.; Yu, R.; Arends, Mark J.; Chandrasekaran, G.; Broecker, V.; Wei, W.; Liu, L.; Swenberg, James A.; Crossan, Gerry P.; Patel, Ketan J., Endogenous Formaldehyde Is a Hematopoietic Stem Cell Genotoxin and Metabolic Carcinogen. *Mol. Cell* **2015,** *60* (1), 177-188.
3. Lai, Y.; Yu, R.; Hartwell, H. J.; Moeller, B. C.; Bodnar, W. M.; Swenberg, J. A., Measurement of Endogenous versus Exogenous Formaldehyde–Induced DNA–Protein Crosslinks in Animal Tissues by Stable Isotope Labeling and Ultrasensitive Mass Spectrometry. *Cancer Res.* **2016,** *76* (9), 2652.
4. Casanova, M.; d'A. Heck, H.; Everitt, J. I.; Harrington, W. W.; Popp, J. A., Formaldehyde concentrations in the blood of rhesus monkeys after inhalation exposure. *Food Chem. Toxicol.* **1988,** *26* (8), 715-716.
5. Tong, Z.; Luo, W.; Wang, Y.; Yang, F.; Han, Y.; Li, H.; Luo, H.; Duan, B.; Xu, T.; Maoying, Q.; Tan, H.; Wang, J.; Zhao, H.; Liu, F.; Wan, Y., Tumor Tissue-Derived Formaldehyde and Acidic Microenvironment Synergistically Induce Bone Cancer Pain. *PLOS ONE* **2010,** *5* (4), e10234.
6. Zhou, X.; Lee, S.; Xu, Z.; Yoon, J., Recent Progress on the Development of Chemosensors for Gases. *Chem. Rev.* **2015,** *115* (15), 7944-8000.
7. Xu, H.; Li, Q.; Wang, L.; He, Y.; Shi, J.; Tang, B.; Fan, C., Nanoscale optical probes for cellular imaging. *Chem. Soc. Rev.* **2014,** *43* (8), 2650-2661.

8. Zhang, R.; Song, B.; Yuan, J., Bioanalytical methods for hypochlorous acid detection: Recent advances and challenges. *TrAC Trends Anal. Chem.* **2018,** *99*, 1-33.
9. Aron, A. T.; Reeves, A. G.; Chang, C. J., Activity-based sensing fluorescent probes for iron in biological systems. *Curr. Opin. Chem. Biol.* **2018,** *43*, 113-118.
10. Jang, Y. J.; Kim, K.; Tsay, O. G.; Atwood, D. A.; Churchill, D. G., Update 1 of: Destruction and Detection of Chemical Warfare Agents. *Chem. Rev.* **2015,** *115* (24), PR1-PR76.
11. Singha, S.; Jun, Y. W.; Bae, J.; Ahn, K. H., Ratiometric Imaging of Tissue by Two-Photon Microscopy: Observation of a High Level of Formaldehyde around Mouse Intestinal Crypts. *Anal. Chem.* **2017,** *89* (6), 3724-3731.
12. Zhao, X.; Ji, C.; Ma, L.; Wu, Z.; Cheng, W.; Yin, M., An Aggregation-Induced Emission-Based "Turn-On" Fluorescent Probe for Facile Detection of Gaseous Formaldehyde. *ACS Sens.* **2018,** *3* (10), 2112-2117.
13. Yang, X.; He, L.; Xu, K.; Yang, Y.; Lin, W., A turn-on fluorescent formaldehyde probe regulated by combinational PET and ICT mechanisms for bioimaging applications. *Anal. Meth.* **2018,** *10* (25), 2963-2967.
14. Bruemmer, K. J.; Green, O.; Su, T. A.; Shabat, D.; Chang, C. J., Chemiluminescent Probes for Activity-Based Sensing of Formaldehyde Released from Folate Degradation in Living Mice. *Angew. Chem. Int. Ed.* **2018,** *57* (25), 7508-7512.
15. Li, J.-B.; Wang, Q.-Q.; Yuan, L.; Wu, Y.-X.; Hu, X.-X.; Zhang, X.-B.; Tan, W., A two-photon fluorescent probe for bio-imaging of formaldehyde in living cells and tissues. *Analyst* **2016,** *141* (11), 3395-3402.
16. Lee, Y. H.; Tang, Y.; Verwilst, P.; Lin, W.; Kim, J. S., A biotin-guided formaldehyde sensor selectively detecting endogenous concentrations in cancerous cells and tissues. *Chem. Commun.* **2016,** *52* (75), 11247-11250.
17. Brewer, T. F.; Chang, C. J., An Aza-Cope Reactivity-Based Fluorescent Probe for Imaging Formaldehyde in Living Cells. *J. Am. Chem. Soc.* **2015,** *137* (34), 10886-10889.
18. Bruemmer, K. J.; Walvoord, R. R.; Brewer, T. F.; Burgos-Barragan, G.; Wit, N.; Pontel, L. B.; Patel, K. J.; Chang, C. J., Development of a General Aza-Cope Reaction Trigger Applied to Fluorescence Imaging of Formaldehyde in Living Cells. *J. Am. Chem. Soc.* **2017,** *139* (15), 5338-5350.
19. Roth, A.; Li, H.; Anorma, C.; Chan, J., A Reaction-Based Fluorescent Probe for Imaging of Formaldehyde in Living Cells. *J. Am. Chem. Soc.* **2015,** *137* (34), 10890-10893.
20. Yang, X.; He, L.; Xu, K.; Yang, Y.; Lin, W., The development of an ICT-based formaldehyde-responsive fluorescence turn-on probe with a high signal-to-noise ratio. *New J. Chem.* **2018,** *42* (15), 12361-12364.
21. Xie, Z.; Yin, B.; Shen, J.; Hong, D.; Zhu, L.; Ge, J.; Zhu, Q., A dual functional fluorogenic probe for visualization of intracellular pH and formaldehyde with distinct fluorescence signals. *Org. Biomol. Chem.* **2018,** *16* (25), 4628-4632.
22. Li, Z.; Xu, Y.; Zhu, H.; Qian, Y., Imaging of formaldehyde in plants with a ratiometric fluorescent probe. *Chem. Sci.* **2017,** *8* (8), 5616-5621.
23. Brewer, T. F.; Burgos-Barragan, G.; Wit, N.; Patel, K. J.; Chang, C. J., A 2-aza-Cope reactivity-based platform for ratiometric fluorescence imaging of formaldehyde in living cells. *Chem. Sci.* **2017,** *8* (5), 4073-4081.
24. Han, B.; Sun, J.; Chen, K.; Chen, Z.; Huang, M.; Gao, Z.; Hou, X., A novel fluorescent probe for formaldehyde based-on monomer-excimer conversion and its imaging in live cells. *Tetrahedron* **2018,** *74* (50), 7193-7197.
25. Liang, X. G.; Chen, B.; Shao, L. X.; Cheng, J.; Huang, M. Z.; Chen, Y.; Hu, Y. Z.; Han, Y. F.; Han, F.; Li, X., A Fluorogenic Probe for Ultrafast and Reversible Detection of Formaldehyde in Neurovascular Tissues. *Theranostics* **2017,** *7* (8), 2305-2313.
26. Nandi, S.; Sharma, E.; Trivedi, V.; Biswas, S., Metal–Organic Framework Showing Selective and Sensitive Detection of Exogenous and Endogenous Formaldehyde. *Inorg. Chem.* **2018**.
27. Li, P.; Zhang, D.; Zhang, Y.; Lu, W.; Wang, W.; Chen, T., Ultrafast and Efficient Detection of Formaldehyde in Aqueous Solutions Using Chitosan-based Fluorescent Polymers. *ACS Sens.* **2018,** *3* (11), 2394-2401.
28. Bi, A.; Gao, T.; Cao, X.; Dong, J.; Liu, M.; Ding, N.; Liao, W.; Zeng, W., A novel naphthalimide-based probe for ultrafast, highly selective and sensitive detection of formaldehyde. *Sens. Actuator B-Chem.* **2018,** *255*, 3292-3297.
29. Cao, T.; Gong, D.; Han, S.-C.; Iqbal, A.; Qian, J.; Liu, W.; Qin, W.; Guo, H., BODIPY-based fluorescent sensor for imaging of endogenous formaldehyde in living cells. *Talanta* **2018,** *189*, 274-280.
30. He, L.; Yang, X.; Ren, M.; Kong, X.; Liu, Y.; Lin, W., An ultra-fast illuminating fluorescent probe for monitoring formaldehyde in living cells, shiitake mushrooms, and indoors. *Chem. Commun.* **2016,** *52* (61), 9582-9585.
31. Tang, Y.; Kong, X.; Xu, A.; Dong, B.; Lin, W., Development of a Two-Photon Fluorescent Probe for Imaging of Endogenous Formaldehyde in Living Tissues. *Angewan. Chem. Int. Ed.* **2016,** *55* (10), 3356-3359.
32. Xu, H.; Xu, H.; Ma, S.; Chen, X.; Huang, L.; Chen, J.; Gao, F.; Wang, R.; Lou, K.; Wang, W., Analyte Regeneration Fluorescent Probes for Formaldehyde Enabled by Regiospecific Formaldehyde-Induced Intramolecularity. *J. Am. Chem. Soc.* **2018,** *140* (48), 16408-16412.
33. Xie, X.; Tang, F.; Shangguan, X.; Che, S.; Niu, J.; Xiao, Y.; Wang, X.; Tang, B., Two-photon imaging of formaldehyde in live cells and animals utilizing a lysosome-targetable and acidic pH-activatable fluorescent probe. *Chem. Commun.* **2017,** *53* (48), 6520-6523.
34. Tang, Y.; Kong, X.; Liu, Z.-R.; Xu, A.; Lin, W., Lysosome-Targeted Turn-On Fluorescent Probe for Endogenous Formaldehyde in Living Cells. *Anal. Chem.* **2016,** *88* (19), 9359-9363.
35. Yuan, L.; Wang, L.; Agrawalla, B. K.; Park, S.-J.; Zhu, H.; Sivaraman, B.; Peng, J.; Xu, Q.-H.; Chang, Y.-T., Development of Targetable Two-Photon Fluorescent Probes to Image Hypochlorous Acid in Mitochondria and Lysosome in Live Cell and Inflamed Mouse Model. *J. Am. Chem. Soc.* **2015,** *137* (18), 5930-5938.
36. Zhu, B.; Li, P.; Shu, W.; Wang, X.; Liu, C.; Wang, Y.; Wang, Z.; Wang, Y.; Tang, B., Highly Specific and Ultrasensitive Two-Photon Fluorescence Imaging of Native HOCl in Lysosomes and Tissues Based on Thiocarbamate Derivatives. *Anal. Chem.* **2016,** *88* (24), 12532-12538.
37. Gao, Q.; Zhang, W.; Song, B.; Zhang, R.; Guo, W.; Yuan, J., Development of a Novel Lysosome-Targeted Ruthenium(II) Complex for Phosphorescence/Time-Gated Luminescence Assay of Biothiols. *Anal. Chem.* **2017,** *89* (8), 4517-4524.
38. Jun, Y. W.; Wang, T.; Hwang, S.; Kim, D.; Ma, D.; Kim, K. H.; Kim, S.; Jung, J.; Ahn, K. H., A Ratiometric Two-Photon Fluorescent Probe for Tracking Lysosomal ATP: Direct In Cellulo Observation of Lysosomal Membrane Fusion Processes. *Angew. Chem. Int. Ed.* **2018,** *57* (32), 10142-10147.
39. Du, Z.; Song, B.; Zhang, W.; Duan, C.; Wang, Y.-L.; Liu, C.; Zhang, R.; Yuan, J., Quantitative Monitoring and Visualization of Hydrogen Sulfide In Vivo Using a Luminescent Probe Based on a Ruthenium(II) Complex. *Angew. Chem. Int. Ed.* **2018,** *57* (15), 3999-4004.
40. Cao, L.; Zhang, R.; Zhang, W.; Du, Z.; Liu, C.; Ye, Z.; Song, B.; Yuan, J., A ruthenium(II) complex-based lysosome-targetable multisignal chemosensor for in vivo detection of hypochlorous acid. *Biomaterials* **2015,** *68*, 21-31.
41. Zhang, F.; Liang, X.; Zhang, W.; Wang, Y.-L.; Wang, H.; Mohammed, Y. H.; Song, B.; Zhang, R.; Yuan, J., A unique iridium(III) complex-based chemosensor for multi-signal detection and multi-channel imaging of hypochlorous acid in liver injury. *Biosens. Bioelectron.* **2017,** *87*, 1005-1011.
42. Zhang, W.; Zhang, F.; Wang, Y.-L.; Song, B.; Zhang, R.; Yuan, J., Red-Emitting Ruthenium(II) and Iridium(III) Complexes as Phosphorescent Probes for Methylglyoxal in Vitro and in Vivo. *Inorg. Chem.* **2017,** *56* (3), 1309-1318.
43. Zhang, W.; Liu, Y.; Gao, Q.; Liu, C.; Song, B.; Zhang, R.; Yuan, J., A ruthenium(ii) complex–cyanine energy transfer scaffold based luminescence probe for ratiometric detection and imaging of

mitochondrial peroxynitrite. *Chem. Commun.* **2018,** *54* (97), 13698-13701.
44. Leung, C.-H.; Zhong, H.-J.; Yang, H.; Cheng, Z.; Chan, D. S.-H.; Ma, V. P.-Y.; Abagyan, R.; Wong, C.-Y.; Ma, D.-L., A Metal-Based Inhibitor of Tumor Necrosis Factor-α. *Angew. Chem. Int. Ed.* **2012,** *51* (36), 9010-9014.
45. Burke, C. S.; Byrne, A.; Keyes, T. E., Highly Selective Mitochondrial Targeting by a Ruthenium(II) Peptide Conjugate: Imaging and Photoinduced Damage of Mitochondrial DNA. *Angew. Chem. Int. Ed.* **2018,** *57* (38), 12420-12424.
46. Burke, C. S.; Byrne, A.; Keyes, T. E., Targeting Photoinduced DNA Destruction by Ru(II) Tetraazaphenanthrene in Live Cells by Signal Peptide. *J. Am. Chem. Soc.* **2018,** *140* (22), 6945-6955.
47. Gill, M. R.; Garcia-Lara, J.; Foster, S. J.; Smythe, C.; Battaglia, G.; Thomas, J. A., A ruthenium(II) polypyridyl complex for direct imaging of DNA structure in living cells. *Nat. Chem.* **2009,** *1*, 662.
48. Zhang, K. Y.; Gao, P.; Sun, G.; Zhang, T.; Li, X.; Liu, S.; Zhao, Q.; Lo, K. K.-W.; Huang, W., Dual-Phosphorescent Iridium(III) Complexes Extending Oxygen Sensing from Hypoxia to Hyperoxia. *J. Am. Chem. Soc.* **2018,** *140* (25), 7827-7834.
49. Huang, H.; Yu, B.; Zhang, P.; Huang, J.; Chen, Y.; Gasser, G.; Ji, L.; Chao, H., Highly Charged Ruthenium(II) Polypyridyl Complexes as Lysosome-Localized Photosensitizers for Two-Photon Photodynamic Therapy. *Angew. Chem. Int. Ed.* **2015,** *54* (47), 14049-14052.
50. Zhou, Z.; Liu, J.; Rees, T. W.; Wang, H.; Li, X.; Chao, H.; Stang, P. J., Heterometallic Ru–Pt metallacycle for two-photon photodynamic therapy. *Proc. Nat. Acad. Sci.* **2018,** *115* (22), 5664-5669.
51. Li, C.; Yu, M.; Sun, Y.; Wu, Y.; Huang, C.; Li, F., A Nonemissive Iridium(III) Complex That Specifically Lights-Up the Nuclei of Living Cells. *J. Am. Chem. Soc.* **2011,** *133* (29), 11231-11239.
52. Ma, D.-L.; Xu, T.; Chan, D. S. H.; Man, B. Y. W.; Fong, W.-F.; Leung, C.-H., A highly selective, label-free, homogenous luminescent switch-on probe for the detection of nanomolar transcription factor NF-kappaB. *Nucleic Acids Res.* **2011,** *39* (10), e67-e67.
53. Yang, G.-J.; Wang, W.; Mok, S. W. F.; Wu, C.; Law, B. Y. K.; Miao, X.-M.; Wu, K.-J.; Zhong, H.-J.; Wong, C.-Y.; Wong, V. K. W.; Ma, D.-L.; Leung, C.-H., Selective Inhibition of Lysine-Specific Demethylase 5A (KDM5A) Using a Rhodium(III) Complex for Triple-Negative Breast Cancer Therapy. *Angew. Chem. Int. Ed.* **2018,** *57* (40), 13091-13095.
54. Sreedharan, S.; Gill, M. R.; Garcia, E.; Saeed, H. K.; Robinson, D.; Byrne, A.; Cadby, A.; Keyes, T. E.; Smythe, C.; Pellett, P.; Bernardino de la Serna, J.; Thomas, J. A., Multimodal Super-resolution Optical Microscopy Using a Transition-Metal-Based Probe Provides Unprecedented Capabilities for Imaging Both Nuclear Chromatin and Mitochondria. *J. Am. Chem. Soc.* **2017,** *139* (44), 15907-15913.
55. Mindell, J. A., Lysosomal Acidification Mechanisms. *Annu. Rev. Physiol.* **2012,** *74* (1), 69-86.
56. Tulpule, K.; Dringen, R., Formaldehyde in brain: an overlooked player in neurodegeneration? *J. Neurochem.* **2013,** *127* (1), 7-21.

SYNOPSIS TOC